Available online at www.sciencedirect.com

ScienceDirect

Underground Space 17 (2024) 132–145

www.keaipublishing.com/undsp

Research Paper

# Real-time estimation of the structural utilization level of segmental tunnel lining

Nicola Gottardi [a,*], Steffen Freitag [b], Günther Meschke [a]

[a] *Institute for Structural Mechanics, Ruhr University Bochum, Bochum 44801, Germany*
[b] *Institute for Structural Analysis, Karlsruhe Institute of Technology, Karlsruhe 76131, Germany*

Received 24 May 2023; received in revised form 11 October 2023; accepted 5 November 2023
Available online 26 January 2024

**Abstract**

Over the last decades, an expansion of the underground network has been taking place to cope with the increasing amount of moving people and freight. As a consequence, it is of vital importance to guarantee the full functionality of the tunnel network by means of preventive maintenance and the monitoring of the tunnel lining state over time. A new method has been developed for the real-time prediction of the utilization level in tunnel segmental linings based on input monitoring data. The new concept is founded on a framework, which encompasses an offline and an online stage. In the former, the generation of feedforward neural networks is accomplished by employing synthetically produced data. Finite element simulations of the lining structure are conducted to analyze the structural response under multiple loading conditions. The scenarios are generated by assuming ranges of variation of the model input parameters to account for the uncertainty due to the not fully determined in situ conditions. Input and target quantities are identified to better assess the structural utilization of the lining. The latter phase consists in the application of the methodological framework on input monitored data, which allows for a real-time prediction of the physical quantities deployed for the estimation of the lining utilization. The approach is validated on a full-scale test of segmental lining, where the predicted quantities are compared with the actual measurements. Finally, it is investigated the influence of artificial noise added to the training data on the overall prediction performances and the benefits along with the limits of the concept are set out.

*Keywords:* Segmental lining; Artificial neural networks; Structural utilization level; Real-time prediction; Structural health monitoring; Monitoring data

## 1 Introduction

The continuous expansion of the underground network and the necessity of maintaining the already existing tunnels in operation require the deployment of strategies to guarantee that the safety and the operability of the underground structures are guaranteed. Concerning deep and long tunnels realized with segmental lining, monitoring measurements play an important role in providing continuous information about the state of the tunnel in terms of structural integrity. However, the capability of interpreting the measurements is crucial to extract valuable information to infer the conditions of the lining structure.

The back analysis is one possible approach for the estimation of the utilization level of the structure since it can be used to reconstruct the stress–strain conditions in the segments starting from available monitored data to detect possible anomalies, as it is explained in (Do et al., 2014; Fabozzi, Bilotta, & Russo, 2017). In the performed study, stresses and radial displacements at specific locations are used as input parameters for the estimation of the lining utilization level. Back analyses are often addressed in geotechnics and geomechanics by different approaches, see Cividini et al. (1981). A pioneering work in this direction is reported in Gioda and Maier (1980), where an inverse problem consisting in the identification of the

* Corresponding author.
*E-mail address:* nicola.gottardi@rub.de (N. Gottardi).
Peer review under the responsibility of Tongji University.

https://doi.org/10.1016/j.undsp.2023.11.011
2467-9674/© 2024 Tongji University. Publishing services by Elsevier B.V. on behalf of KeAi Communications Co. Ltd.
This is an open access article under the CC BY-NC-ND license (http://creativecommons.org/licenses/by-nc-nd/4.0/).

parameters of an elastoplastic ground using search algorithms is worked out. In Sakurai (2017), four main levels of back analyses are identified for tunnels in rock for the estimation of the rock mass parameters. The first is based on the pure inversion of the analytical formulations describing the behavior of the rock mass and its interaction with the tunnel lining. However, this approach is feasible only for simple engineering problems, for which analytical solutions exist. A second and simpler effective approach is the direct method, which is based on the solution of a minimization problem. This consists in minimizing the discrepancy between the recorded measurements and their respective values in the numerical analyses, to obtain the optimal match for the given measured data (for more details see Sakurai (2017)). Another method encompasses probabilistic approaches, which include uncertainty and provide an estimation of the sought parameters in terms of mean and variance. An example is the Bayesian approach, wherein a priori knowledge is introduced to restrict the input space of the rock mass parameters. Finally, inverse problems can be addressed also using the Fuzzy Set Theory, since a priori knowledge can be introduced to help to construct a probability density function for the rock mass parameters, or using machine learning algorithms, like artificial neural networks, which can deal with many input parameters.

A further interesting approach for the structural analysis of segmental tunnel lining based on analytical solutions of the curved beam is the hybrid method proposed by Zhang et al. (2017), where deformations and stress resultants can be computed given a certain load. Applications of the method to a bridge and an arched-like structure are presented in Zhang et al. (2020), while extensions of the method to account for a load due to the in situ stress, the nonlinear behavior at the joints and the long-term creep effects of a tunnel lining are set out (Zhang et al., 2019; Hellmich et al., 2020).

The deployment of machine learning tools in underground constructions, such as artificial neural networks (ANN), represents a flexible way that permits to identify relationships between input quantities and the ones designated as targets, i.e., the quantities which need to be identified. Applications of machine learning in underground construction for the analyses of surface settlements and building damage induced by mechanized tunneling are illustrated (Cao et al., 2022; Saadallah et al., 2019; Erharter et al., 2019). While radial displacements and circumferential stresses at specific monitoring locations in the lining are chosen as input variables in this work, stresses at positions where no sensors were applied are selected as outputs. ANNs are inspired by the biological brain and are considered universal approximators capable of dealing with highly nonlinear problems (Bishop, 2006; Haykin, 1999; Basheer & Hajmeer, 2000). They have been applied successfully in many fields of structural mechanics (Freitag, 2015), both for system identification and structural health monitoring. An overview of the application of ANNs in civil engineering problems is given also in Adeli (2001), where applications for structural control and monitoring of structures are presented.

In this study, it is investigated the deployment of ANNs to achieve real-time predictions of the utilization level of the lining based on given input measurements. For the construction of the machine learning algorithm, synthetic data generated using finite element models are employed. A similar approach for the real-time estimation of the maximum bending moment in a beam structure based on monitored displacements at three locations is presented in Gottardi et al. (2023b), where the focus is on the correlation between input parameters resulting from an analytical model used to train the ANN. In this case, artificial noise is added to the synthetic ANN training data to bridge the discrepancy between the real system and the simulation model.

Here, the methodological approach developed for segmental tunnel lining is validated on a full-scale ring test (Blom & van Oosterhout, 2001; Blom, 2002), where the predictions of the ANNs are compared with additional monitored values in the lining. To explore the influence of white noise on the prediction performances of the ANNs, a similar approach as used in Gottardi et al. (2023b) is applied for the tunnel lining stress prediction.

## 2 Concept for the stress–strain state assessment in segmental tunnel linings

To cope with the necessity of dealing with the great number of underground infrastructures, where safety and serviceability conditions need to be constantly guaranteed, a new concept which considers monitored quantities in the tunnel for the estimation of the utilization level is developed. The main goal consists in exploiting available measurements from the tunnel lining, e.g., displacement or strain measurements, by means of a method, which is capable of providing in real-time the assessment of the target quantities, such as the maximum stress state reached in the structure, to estimate the structural utilization of the lining. To generalize the applicability of the method, it is developed by taking into account multiple kinds of possible input measurements, which depend on the configuration of the monitoring section installed in the lining.

The method consists of two main steps, an online and an offline phase (see Fig. 1). While in the former the monitored data are given as input to the algorithm for the estimation of the target quantities, the latter includes the construction of the algorithm itself through FE analyses of the structure and the selection of the most suitable machine learning model. A pivotal role is played by the FE models, which are employed for the analyses of manifold scenarios and are required to produce the synthetic data needed for the training of the ANNs. In this study, only synthetic data are used during training, in order to develop a framework based exclusively on the physics reproduced by the FE analyses. If abundant measurements are available, they can also be included in the training

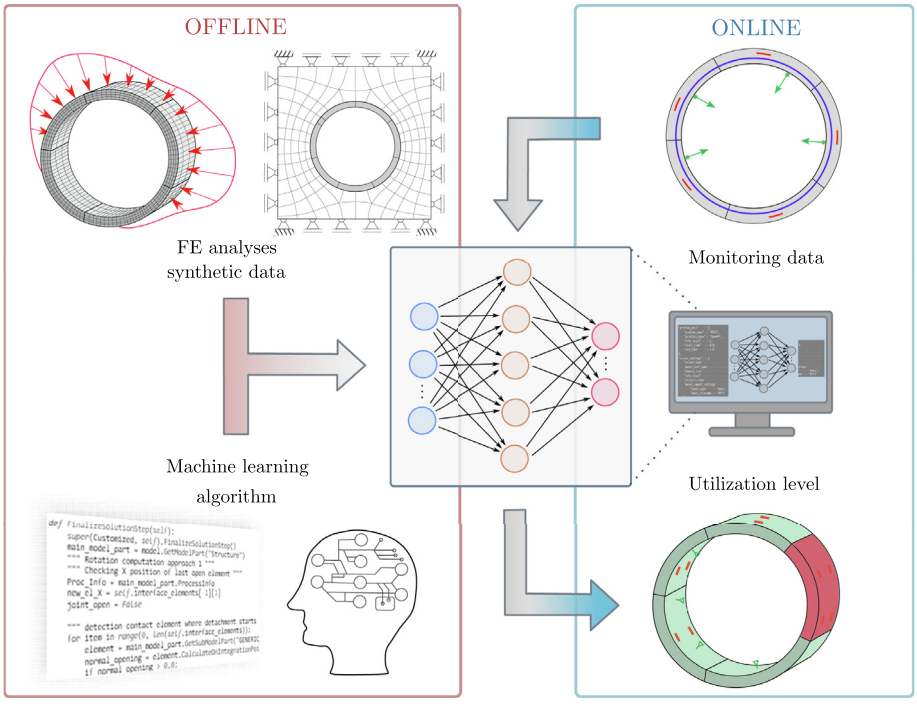


Fig. 1. Diagram representing the methodological approach with offline and online phase.

process, but these could not be applied to the case at hand. The type of neural networks used here are feedforward neural networks (FNNs). These metamodels are valuable tools for data mining and for real-time predictions of the target quantities to be determined for the structural health evaluation of the tunnel lining.

The advantage of this methodological approach is the use of the available measured data to acquire information about the system object of investigation and to increase therefore our knowledge about its integrity. Using the estimation of the maximum stress–strain state in the lining, it is possible to plan in advance maintenance interventions and detect anomalies over the life of the structure, if continuous monitoring is performed. This digital approach for structural health monitoring of underground structures allows for a safer and more sustainable manner to monitor the state of the segmental lining, since the monitored data can be analyzed off-site.

The presented concept is validated with a full-scale experiment consisting of three segmental lining rings subject to non-uniform radial loads, where the stresses predicted by the algorithm are compared with the ones measured in a real lab test.

## 3 Full-scale lining test

The developed approach for the structural utilization level assessment of the lining is validated on a full-scale test (Blom & van Oosterhout, 2001; Blom, 2002) performed at the Stevin laboratory in Delft. It consists of three segmental rings of the type of the ones employed in the Botlek Rail Tunnel (BRT), see Fig. 2. The seven reinforced concrete (RC) segments are assembled vertically one upon the other in a staggered way so that the self-weight can be neglected when evaluating its behavior under radial loads. The base ring is placed on Teflon layers, to reduce the friction, and it is additionally restrained with four tangential guided slides every 90° to avoid rigid body motions. Rigid motions of the ensemble might happen due to slight misalignments of the radial jacks.

The ring is loaded by the jacks in three steps. First, confinement in the vertical direction is performed by an axial load acting on the uppermost ring. Afterward, a second confinement is applied by radial pressure to achieve a full contact state for the segments, while finally, the lining is subject to a deviatoric load inducing an ovalization of the ring. The parameters of the experimental setup are reported in Table 1. Regarding the measurements taken during the test, the lining inner radial displacements were densely recorded, while the stresses were measured at positions $\varphi = 26°, 77°, 129°, 179°, 231°, 276°$ and 289° in the segments (see Fig. 4).

The strain gauges are attached to the upper and lower reinforcement layers and measure the strains in the circumferential direction. The concrete cover of the rebars is $c' = 50$ mm, therefore knowing the cross-section height $t$ and assuming a linear elastic behavior, it is possible to compute the equivalent stress at the segment surface (see Fig. 4). All the readings were carried out at the final stage of the loading process.

## 4 Finite element model

For the training of FNNs, a data set is required, which can be either constituted by monitored data or by synthetic

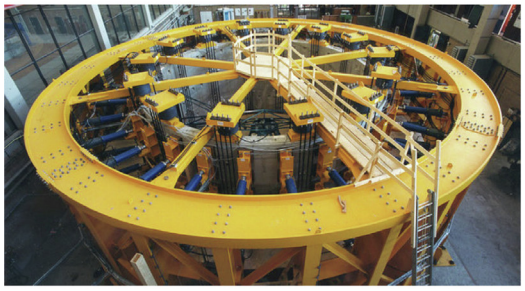

(a)

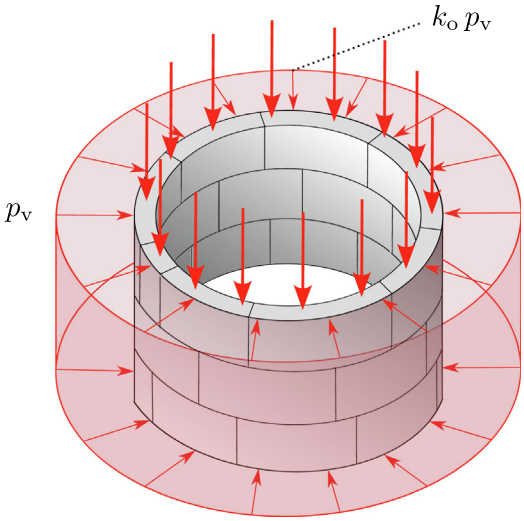


(b)

Fig. 2. Full-scale test setup. (a) Image of the test, and (b) load scheme of the test setup.

Table 1
Parameters of the full-scale test on the segmental lining conducted at TU Delft (Blom & van Oosterhout, 2001; Blom, 2002).

| | Parameter | | Value | Unit |
|---|---|---|---|---|
| RC | Young's modulus | $E$ | 40.0 | GPa |
| | Poisson's ratio | $\nu$ | 0.2 | – |
| | Thickness | $t$ | 0.4 | m |
| | Concrete cover | $c\prime$ | 0.05 | m |
| | Inner radius | $r_{inn}$ | 4.325 | m |
| | Outer radius | $r_{out}$ | 4.725 | m |
| | Ring width | $b$ | 1.5 | m |
| Load | hydrostatic load | $p_0$ | 429.5 | kPa |
| | deviatoric load | $q_0$ | 18.5 | kPa |

data. Within the scope of the developed method, the data set used for the generation of the FNN is obtained by finite element (FE) analyses of the tunnel lining under consideration.

In the FE model, the segmental lining is embedded in an elastic continuum representing the hosting rock mass and assuming a plane strain state (see Fig. 4). The actual boundary conditions of the experiment are not replicated in the model since the aim is to create scenarios that are not covered by the experiment, to make the approach more general and to increase the complexity of the problem to be solved, e.g., unknown loading conditions.

The model is generated in the finite element software for multiphysics analyses KRATOS (Dadvand et al., 2010). The lining is featured with an elastic material and it is represented by considering both the segment geometry and the mutual interaction among them and the surrounding ground. The joints between the segments are accurately reproduced by deploying interface elements, which allow for relative rotations between the segments and, as a consequence, the structural kinematics. This particular kind of elements, which are zero-thickness elements, are capable of modeling the interaction between model parts according to user-defined constitutive laws (Snozzi & Molinari, 2013; Schäfer et al., 2021; Gudzulic et al., 2020). For the case at hand, a non-cohesive simple frictional law has been chosen to characterize the lining joints, where the term non-cohesive is to be intended so that no tensile stresses occur when the joints open. Since among the segment joints, the interaction is between concrete to concrete surfaces, the corresponding friction coefficient $\mu$ is used to characterize the Coulomb friction law, defined as

$$\tau = \mu \cdot \|\sigma_n\|, \tag{1}$$

with $\sigma_n$ being the normal stress component to the surface and $\tau$ the tangential one. Conversely, the interaction between the lining and the elastic bedding is modeled using a simple-cohesive law, where the cohesion (i.e., the interface tensile strength) is set to a very small value to stabilize the numerical model. For more details on the parameters used in the model see Table 2. The segments are modeled with elastic material since the stresses remain in the elastic range in the experiment and the tensile strength of the concrete is not reached.

The model domain is constrained along its boundaries, according to the hypothesis of deep tunnels, and is characterized by a geostatic stress applied in the form of prestress directly in the hosting continuum (see Fig. 3). A further

Table 2
Parameters of the joints between the lining segments and the interfaces between the lining and the bedding material used in the FE model (Blom & van Oosterhout, 2001).

| Interface | Parameter | | Value | Unit |
|---|---|---|---|---|
| Inter segment | Friction coefficient | $\mu$ | 0.4 | – |
| | Contact width | $w_c$ | 170 | mm |
| Lining-ground | Friction coefficient | $\mu$ | 0.0 | – |
| | Tensile strength | $f_t$ | $10^{-5}$ | MPa |

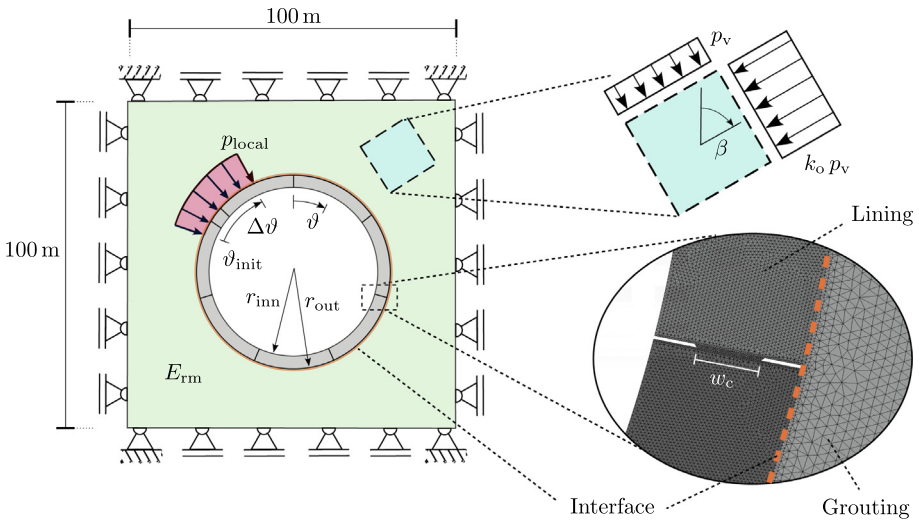


Fig. 3. FE model used for the generation of the synthetic data set.

assumption in the analysis of deep tunnels is that the lithostatic stress state can be assumed to be constant in the domain, as its variation with changing depth is usually negligible. The use of elastic behavior for the ground makes this model very similar to the representation of the system by means of a bedded beam model, in which springs replace the surrounding ground. However, in bedded beam models, the accurate load transfer between ground and structure is not reproduced, since their interaction is taken into account in a simplified manner.

To consider different loading conditions on the tunnel, another source of load is introduced in the model. Besides the in situ stress, which is governed by the tunnel depth, the rock density and $k_o$, a localized load acting along some portions of the tunnel lining is added, to take into account possible rock wedge detachments, activations of faults or localized swelling phenomena.

In the FE models, the lining is embedded in the hosting rock mass, while in the full-scale lining test, which is used to validate the approach, no actual ground is present as the load is applied to the structure via radial hydraulic jacks in a load-controlled fashion. The reason for modeling the bedding is that in reality, the boundary conditions of the lining are uncertain, since the actual interaction among rock mass, pea gravel and segments cannot be precisely determined. In light of this, the modeling of the bedding is deployed to prove the generality of the method and a real situation where the specific boundary conditions remain partially unknown.

## 5 Sampling procedure

The FE model is being used for the generation of the synthetic data, which are required for the training of the neural networks. To generate such data set, the main input parameters that most affect the FE model response are detected by a sensitivity study and a range of variation for each of them is defined (see Table 3). The Young's modulus of the bedding ground, the vertical component of the geostatic stress, the $k_0$ value and the inclination of the vertical geostatic stress with respect to the vertical direction are firstly listed in Table 3, while the amplitude, the extension and the location of the localized load applied on the lining are shown underneath (see Fig. 3).

Table 3
Ranges of variation of the FE input parameters used during the sampling of the different scenarios.

| | Parameter | | Range | Unit |
|---|---|---|---|---|
| Ground | Young's modulus | $E_{rm}$ | [5.0, 105.0] | MPa |
| In-situ stress | Vertical component | $p_v$ | [0.2, 1.5] | MPa |
| | Stress ratio | $k_0$ | [0.5, 1.1] | – |
| | Stress orientation | $\beta$ | [0, 180.0] | ° |
| Load | Amplitude | $p_{local}$ | [0, 300.0] | kPa |
| | Extension | $\Delta\vartheta$ | [10.0, 80.0] | ° |
| | Position | $\vartheta_{init}$ | [0, 360.0] | ° |

In general applications, analyses of the project reports or engineering judgment can aid in the identification of the parameter intervals. A remarkable source of uncertainty is also related to the load conditions on the segments. For this reason, two kinds of loads are considered in the ground simultaneously, both an in situ stress and a localized load. For the last load type, a range of variation of its amplitude and extension is defined and furthermore, it is assumed that this localized load can act at different positions along the lining.

A Monte Carlo procedure is carried out for the generation of the input parameter sets for the FE analyses, and specifically the Latin hypercube sampling is deployed in the experimental design of the 7-dimensional input space. For the case here investigated, 4000 samples are generated and analyzed with the FE model. The FE results are finally reorganized to build up the training data set for the creation of the FNNs.

## 6 Feedforward neural networks for structural utilization assessment

The approach for the structural utilization estimation of the lining has been developed within a framework, which includes machine learning tools to accomplish the prediction in real-time of the target quantities. Specifically, feedforward neural networks (FNNs) are employed in this study. Multilayer neural networks are universal approximators of any arbitrary function, which find useful application either when no mathematical models are available to describe a phenomenon, but only measured data of it, or when the analytical models are too complex to be solved (Basheer & Hajmeer, 2000).

FNNs are a particular type of neural networks, which are made of multiple layers, where each layer contains multiple neurons. The network is featured with an input layer, some hidden layers and an output layer. The input data are presented to the first FNN layer, where they are normalized in the range $[-1, 1]$ and passed to the neurons of the first hidden layer. Each neuron is linked with the ones of the previous and the following layer. When the signals from the previous layer reach a neuron, these are multiplied each by the synaptic weights, are all summed up and a bias value is added. Afterward, the result is fed to the activation function, which transforms the signal within a certain range. A neuron $k$ is the fundamental processing unit of the network, which transforms the given input signals $x_j$ into a new signal $y_k$, according to the following relation:

$$y_k = \phi\left(\sum_{j=1}^{m} w_{kj}x_j + b_k\right), \tag{2}$$

where $w_{kj}$ are the weights used to multiply each input signal $x_j$, $b_k$ is a bias value, and $\phi$ is the activation function used to transform the signal into a specific range. In this work, the hyperbolic tangent function is chosen as activation function, obtaining:

$$y_k = \tanh\left(\sum_{j=1}^{m} w_{kj}x_j + b_k\right). \tag{3}$$

After the signal has traveled through the network, it is passed to the output layer where it is scaled back to the physical range.

In the proposed method, fully connected FNNs are deployed to learn dependencies among stresses and displacements at monitoring points (input) and stresses at other positions (output). For this study, MATLAB programming environment has been used. The FNN training optimization algorithm selected is Levenberg–Marquardt, where the mean square error on the normalized output is employed as a loss function. The learning rate has been fixed to 0.001. An early-stopping criterion is deployed to avoid overfitting, based on tracking the reduction rate of the loss function both for the training and validation datasets. All the network weights and biases are initiated randomly at the beginning of the training process, therefore multiple networks need to be trained to ensure the repeatability of the generation of metamodels with specific performances.

## 7 Applications and results

For the evaluation of the quantities of interest in the lining, manifold architectures and configurations for the feedforward neural networks are investigated. For the case at hand, the following input–output patterns are considered:

(1) The circumferential stresses at the extrados at the middle cross-section of 5 designated segments (see Fig. 4) are considered as input of the FNN, while the stresses at positions $\varphi = 77°$ and $231°$ represent the quantities to be predicted.
(2) The inner radial displacements of the lining at 6 points ($\varphi = 26°, 77°, 129°, 232°, 289°$, and $340°$) are assumed as input of the FNN, while the circumferential stresses at positions $\varphi = 77°$ and $231°$ are selected as output (see Fig. 4).

The circumferential stresses are adjusted to take into account only the bending contribution. This is carried out by removing from the stresses the component related to axial compression, by assuming a linear distribution of the strains along the cross-section and by the superposition principle.

The choice of the input quantities is based on the feasibility of recording specific measurements on-site in the tunnel, taking into account possible obstacles, which might prevent the monitoring of certain quantities. As for the output, since tensile stresses due to bending can provoke cracking in the lining, the bending stresses are selected as target quantity. However, given the reduced number of stress measurements provided by the test, two positions, wherein the measured bending stresses are the highest, are defined as the locations for the output stresses. Using exclusively the stresses at the positions where they are measured in the real-scale test, enables us to validate the developed method.

If standard-equipped monitoring sections are assumed, the choice of the former configurations is achieved, as it can be seen in Fig. 4. An aspect to be addressed is that the input data, namely the radial displacements as well as the tangential stresses at specific locations of the lining, are correlated with each other. This influences the shape of the training space of the FNN, since the input data (which are results of FE simulations) do not homogeneously distribute in the input space but tend to locate according to certain patterns. For this reason, while applying the model it does not suffice to merely check that the real measurements fall within the boundaries of the training domain, made of the synthetic data, but that the measurements also reflect a similar degree of correlation of the

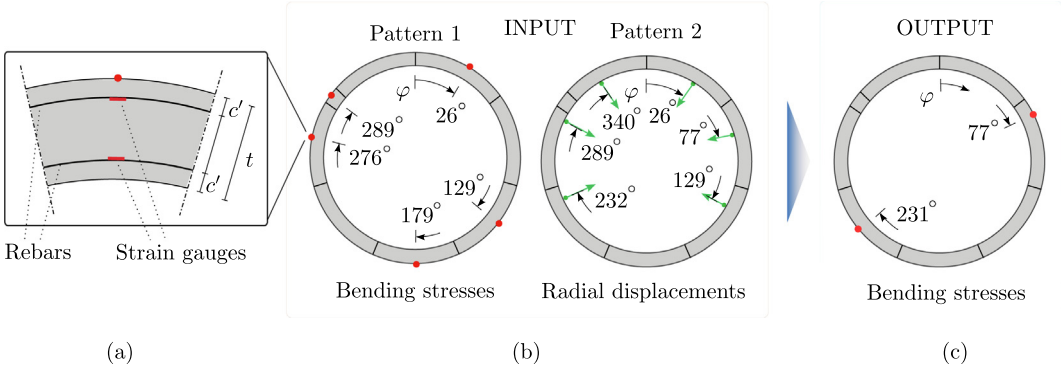


Fig. 4. Input and output of the framework. (a) Zoom of the segment structure, (b) input bending stresses and radial displacements, and (c) predicted stresses.

one of the synthetic data (Gottardi et al., 2023b). With a multidimensional input, it is possible to analyze 2D projections of the input space to visualize the type of correlations among the inputs, as it can be observed in Fig. 5, where an example of the interaction between 3 of the input displacements is shown.

The accuracy of the approach on the synthetic data by using the circumferential stresses as input quantities is firstly addressed. A batch of 10 FNNs is trained and the performances in terms of the mean and standard deviation of the predictions of the networks on the synthetic data, in terms of normalized mean squared error MSE, are analyzed. These indicators are computed for both the training and testing stages. A scheme of the network architecture is provided in Fig. 6, in which inputs, outputs and hidden layers with respective activation functions are depicted, along with the loss function trend over the training epochs obtained for one network of the batch. Of the overall samples, 60% of them were used for the training of the FNNs, while the other 40% for testing, i.e., to verify the performances of the neural network on data not used for the tuning of its hyperparameters. Subsequently, to verify the prediction accuracy in the real scenario of the full-scale test, the average and the standard deviation of the batch network predictions, fed with the real input data, are calculated and compared with the actual measured values of the stresses. To quantitatively determine the quality of the predictions in an average sense, the following relative error estimator $e_{\%,i}$ is computed for both predicted stresses:

$$e_{\%,i} = \frac{\left(\frac{1}{N}\sum_{k=1}^{N}\sigma_{k,i}^{\text{pred}}\right) - \sigma_i^{\text{meas}}}{\sigma_i^{\text{meas}}} \times 100, \tag{4}$$

where $N$ is the number of FNNs trained, in this study equal to 10, $\sigma_{k,i}^{\text{pred}}$ is the predicted bending stress $\sigma_i$ by the neural network $k$, $\sigma_i^{\text{meas}}$ is the measured bending stress in the lab test and $e_{\%,i}$ is the error expressed in percentage. It is worth noting the good accuracy of the network predictions, which achieve on average an error $e_{\%,77}$ of $-0.5\%$ and $e_{\%,231}$ of $3.3\%$ in the estimation of the real stress values, respectively.

The analogous procedure is conducted also for the prediction of the bending stresses at the same locations as before, but employing radial displacements at the positions defined in Fig. 4. Batches of 10 neural networks are generated and the average performances of the network groups

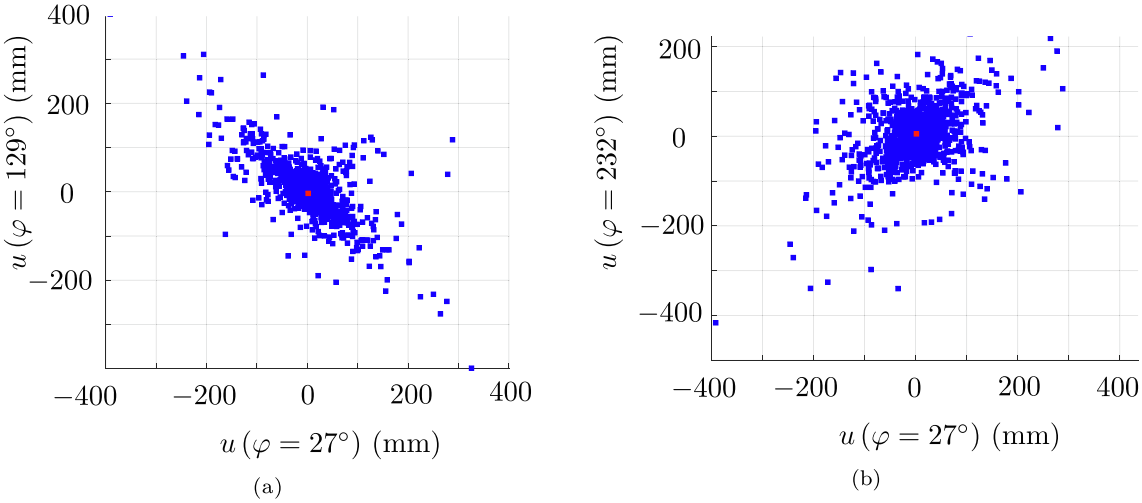


Fig. 5. Correlation between input displacements. (a) Relation between $u(\varphi = 27°)$ and $u(\varphi = 129°)$, and (b) relation between $u(\varphi = 27°)$ and $u(\varphi = 232°)$.

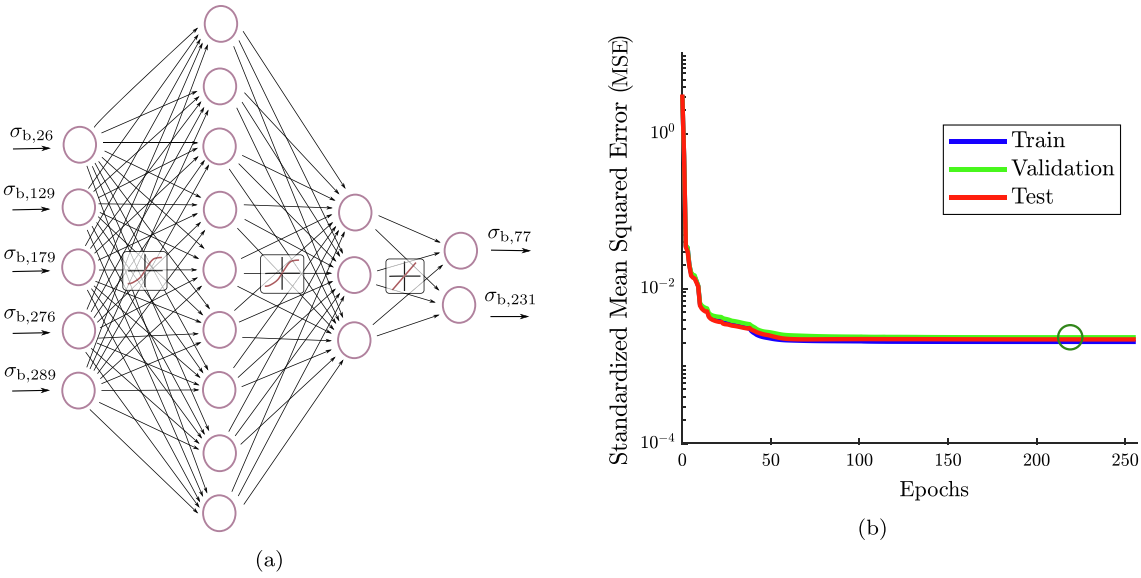


Fig. 6. FNN developed for the framework. (a) Architecture used for pattern 1, and (b) loss function over the training epochs for one network and optimal point.

both on the synthetic scenarios and for the real testing case are computed. The results of the training, validation and testing process of one of the batch network for pattern 2 are illustrated in Fig. 7. The normalized target and network output are plotted against each other in order to verify the success of the training process in its substages, i.e. training, validation and testing. As it can be observed from Fig. 7, the predictions on the synthetic samples are distributed in all three charts nearby the diagonal of the quadrant, which represents a perfect match between predicted and target outputs. The small dispersion of the data signifies a good accuracy of the trained model. Likewise to beforehand, very good accuracy of the predictions for the neural networks are to be observed when they are tested on the measurements of the full-scale test, with errors of −6.5% and 1.5%. The motivation behind the training of multiple neural networks lies in avoiding that models with good performances are obtained by chance, i.e., to get robust FNN models.

The FNN characteristics, their architecture and their performances are summarized in Tables 4 and 5. In the first table, the specific input and output quantities for each pattern are listed in the upper table section, while the average of the normalized MSE and its standard deviation achieved during the training and testing phase on the synthetic scenarios are reported below. Finally, in Table 5, the prediction accuracy of the networks with respect to the measured targets are presented for the patterns 1 and 2. It can be observed that by using stress measurements obtained from the strain gauges more accurate predictions are achieved from the neural networks, than using the displacements as input. This has an advantage from the practical perspective, as strain measurements are more frequently recorded in segmental linings rather than radial displacements.

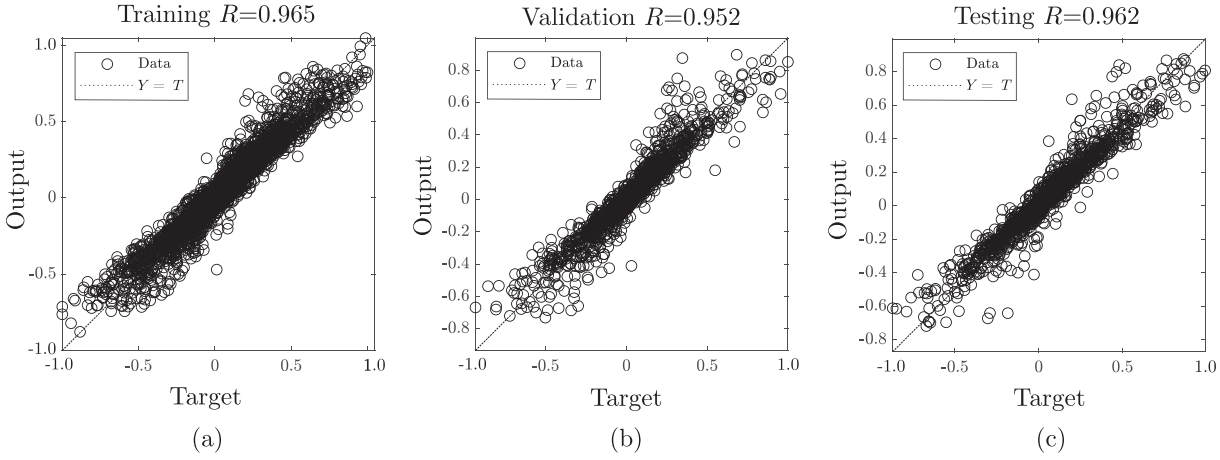


Fig. 7. Performances of one of the neural networks of pattern 2. (a) Training, (b) validation, and (c) testing.

Table 4
Performances exhibited by the FNNs for both patterns 1 and 2 on the synthetic data.

| Pattern | Samples | Arch.[a] | Input [b] | Output | $\mu_{train}$ [c] | $\sigma_{train}$ [c] | $\mu_{test}$ [c] | $\sigma_{test}$ [c] |
|---|---|---|---|---|---|---|---|---|
| Pattern 1 | 4000 | 9–3 | $\sigma_b$ @ 26°, 129°, 179°, 276°, 289° | $\sigma_b$ @ 77°, 231° | $2.04 \times 10^{-3}$ | $8.05 \times 10^{-5}$ | $2.18 \times 10^{-3}$ | $1.61 \times 10^{-4}$ |
| Pattern 2 | 4000 | 10–3 | $u_r$ @ 27°, 77°, 129°, 232°, 286° 340° | $\sigma_b$ @ 77°, 231° | $4.31 \times 10^{-3}$ | $3.47 \times 10^{-4}$ | $6.13 \times 10^{-3}$ | $1.04 \times 10^{-3}$ |

[a] Architecture: neurons in the hidden layers. Each hidden layer is separated by - sign.
[b] The positions of the input data are specified by the angles $\varphi$ following the @ symbol.
[c] Mean and standard deviation of the normalized MSE during training and testing of the FNNs on the synthetic data.

Table 5
Comparison between the mean predicted values and the target bending stresses.

| Pattern | $\mu_{pr}$ (MPa) | $\sigma_{pr}$ (MPa) | $e_{abs}$ (MPa) | $e_{\%}$ (%) | Target (MPa) $\sigma_{b,77}$ | Target (MPa) $\sigma_{b,231}$ |
|---|---|---|---|---|---|---|
| Pattern 1 | 4.894 | $1.60 \times 10^{-1}$ | $-2.80 \times 10^{-2}$ | $-5.63 \times 10^{-1}$ | 4.921 | |
| | 4.834 | $1.38 \times 10^{-1}$ | $1.56 \times 10^{-1}$ | 3.328 | | 4.678 |
| Pattern 2 | 4.601 | $1.41 \times 10^{-1}$ | $-3.20 \times 10^{-1}$ | −6.501 | 4.921 | |
| | 4.747 | $1.66 \times 10^{-1}$ | $6.91 \times 10^{-2}$ | 1.468 | | 4.678 |

### *7.1 FNN prediction capabilities with reduced input measurements*

On the field, it might happen that obstacles arise and originally planned measurements cannot be taken or that some sensors fail over time. In this regard, it is of interest to comprehend if the presented approach can still provide a reliable assessment of the sought quantities $\sigma_{b,77}$ and $\sigma_{b,231}$. A parametric study is undertaken and the prediction capabilities of the models are investigated for a different number of input measurements, considering both patterns 1 and 2. As it can be observed from Fig. 8, when bending stresses are employed as input for the FNN still satisfactory predictions can be obtained with fewer input measurements. Conversely, when $\sigma_{b,77}$ and $\sigma_{b,231}$ are predicted starting from displacements, a reduction of the input measurements for the neural network produces a swift decline in its prediction quality. However, for both patterns, when 2 or fewer input measurements are used, poor training of the neural network is achieved ($R = 0.83$ with 2 inputs, $R = 0.2$ with 1 input), meaning that the models generated are unreliable. It is worth mentioning, that when the input of a FNN is not sufficient for the solution of the problem at hand, this can be reflected by the impossibility of achieving a good training of the model. On the other hand, a good training of the FNN does not necessarily guarantee its goodness. Further details on the measurements used are given in Appendix A.

### *7.2 Artificial noise added to the training data*

The input quantities considered in the method performed can be partially correlated with each other. This translates into a non–homogeneous distribution of the sample points within the training space, since they distribute according to a certain shape in the space due to their correlation. To avoid extrapolation during the application of the neural networks to measured data, it is not sufficient to merely consider the ranges of the training space, and yet it is necessary to compare the correlation of the input measurements with the ones of the training data. In reality, it is difficult to achieve a perfect match in the degree of correlation between the FE model results and the actual measurements due to different types of uncertainty involved, which also regard the intrinsic definition of the employed models (French, 1995).

An innovative method to deal with extrapolation is presented in Gottardi et al. (2023b) where artificial noise is added to the input synthetic data before the training of FNNs, as a strategy to weaken the perfect correlation among the data. The approach was applied to a simple beam and validated with a 4-point bending test. The method was then extended and applied to a tunnel segmental lining and verified using an artificial scenario (Gottardi et al., 2023a).

The aim is to investigate whether the application of noise to the input synthetic data improves the neural network predictions also for the investigated tunnel lining when these data are used for training. The input–output configurations for the FNNs analyzed are the same as reported in Table 4. Several noise levels with a uniform distribution over the determined ranges are defined. Likewise to Section 7, groups of 10 FNNs are generated with similar architecture and layout as beforehand and the mean along with the standard deviation of the predictions of the neural networks of each batch are computed. The results obtained when stresses are employed as input (pattern 1) to predict the bending stress at position $\varphi = 77°$ and $\varphi = 231°$ are visualized in Fig. 9, while for radial displacements as input (pattern 2), the results are depicted in Fig. 10. The mean and the standard deviation of the predicted $\sigma_{b,77}$ and $\sigma_{b,231}$ for the batch corresponding to each noise level are drawn (red and orange lines) against the measured reference value (blue broken line). The noise amplitude is

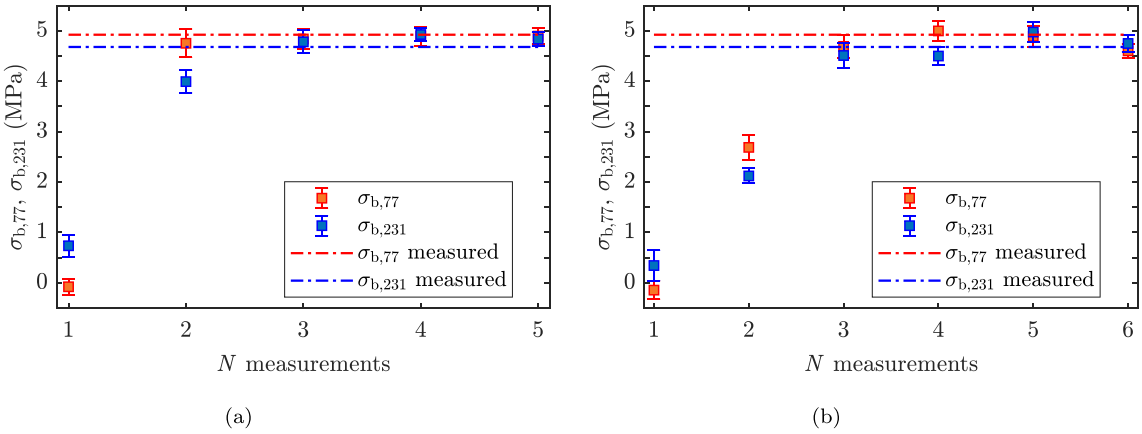


Fig. 8. Predictions of the FNNs of $\sigma_{b,77}$ and $\sigma_{b,231}$ with respect to used input measurements. (a) Results for pattern 1, and (b) for pattern 2.

determined by the value of the maximum $\Delta\sigma$ applied to the the synthetic input data with respect to the average measured stress $\bar{\sigma}$ in the full-scale test.

The stress predictions obtained by batches of FNNs trained with manifold noise levels are not much improved, showing a steady trend for the several noise amplitudes investigated. Also, the standard deviation does not vary significantly and remains narrow, which means that multiple neural networks in each group present similar performances. Such behavior suggests that the original data already provide a good platform for the generation of the FNNs since extrapolation seems not to occur. It is not obtrusive to verify a priori if extrapolation happens in a multidimensional problem, since a visualization of the input space is not possible for more than 3 input dimensions. For this reason, the analysis of the trends of the predicted quantities can provide valuable insight on this issue.

### *7.3 Plausibility checks of the FE model*

The FE model used for the generation of the synthetic data is characterized by plane strain conditions and the presence of a bedding material around the tunnel. In the real experimental setup, however, these assumptions are not completely fulfilled, therefore a plausibility check of the response obtained in the FE model for the lining is carried out. Specifically, it is investigated if the numerical analyses under the former hypotheses can reproduce, for a specific set of input parameters, the behavior of the real system within a certain accuracy. In the experiment, the radial load was applied by radial jacks directly to the lining (in load control), while in the FE models the acting load on the lining results automatically from the lining-bedding interaction. As it is explained in Section 4, the in situ stress is inserted directly into the bedding ground, which deforms exerting a reaction load on the lining. Furthermore, axial jacks were used to apply axial confinement to the three-ring full-scale test. Since in a 2D model, it is not possible to apply a load perpendicularly to its plane, the hypothesis of plane strain conditions is made to take into account the axial imposed load. It is obtrusive that the real test is not in perfect plane strain conditions and therefore this assumption needs also to be verified. The ground parameters of the FE model are tweaked until the radial load transferred from the bedding to the segments is similar in magnitude to the one applied by the hydraulic jacks in the experiment.

The comparison between the results obtained by the FE model and the measured data in the experiment are depicted in Figs. 11 and 12, where both the circumferential bending stresses along the outer surface of the lining and

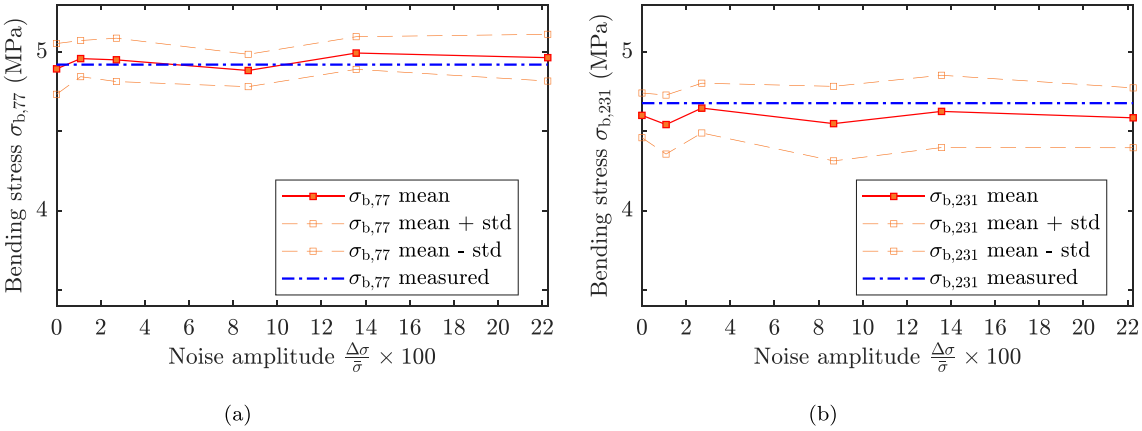


Fig. 9. Performances of the FNN batches for different noise levels. (a) Predicted bending stress $\sigma_{b,77}$, and (b) predicted bending stress $\sigma_{b,231}$.

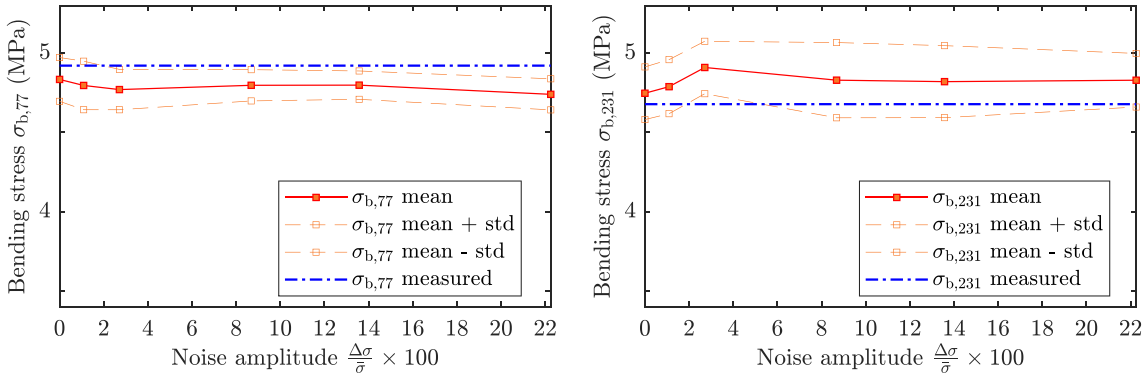


(a) (b)

Fig. 10. Performances of the FNN batches for different noise levels. (a) Predicted bending stress $\sigma_{b,77}$, and (b) predicted bending stress $\sigma_{b,231}$.

the radial inner displacements are depicted. The stresses in the vicinity of the joints are not plotted since in these regions concentrations and localizations of stresses take place, and therefore the bending stresses become meaningless. A good agreement in both cases is obtained, achieving a root mean squared error (RMSE) between the FE predicted stresses and the measured ones equal to 0.346 MPa, while for the displacements RMSE is equal to 0.461 mm. The good match between the measurements recorded during the test and the results gained from the FE analysis reveals that the assumptions introduced in the FE analyses are acceptable.

A further plausibility check is performed by feeding the FNNs trained on the synthetic data for both patterns 1 and 2, with the input values retrieved by the FE analysis here performed. As we can see from the results reported in Table 6, the stresses at the sought locations can be predicted, even though a non-negligible error is obtained. This is caused by the slight deviation between the FE model results and the lining response in the real test.

As final remark, a great advantage of carrying out FE analyses is the possibility to retrieve other kinds of information by querying the FE model for the physical quantities one might be interested in, e.g., maximum stresses recorded in the structure or the stress distributions close to the joints.

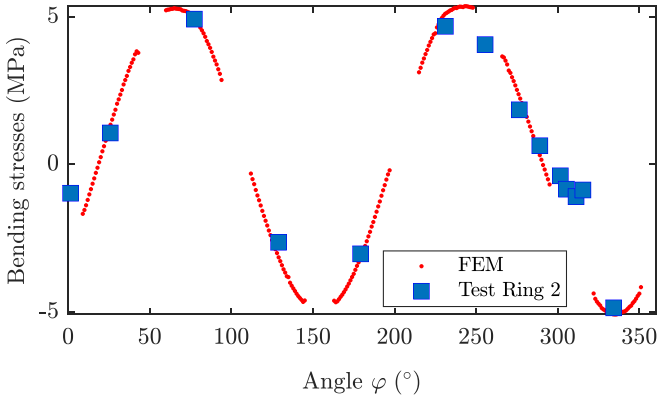


Fig. 11. Comparison between the measurements of the bending stresses along the outer lining surface obtained in the full-scale test (markers in blue) and the ones obtained by the FE analysis (red points).

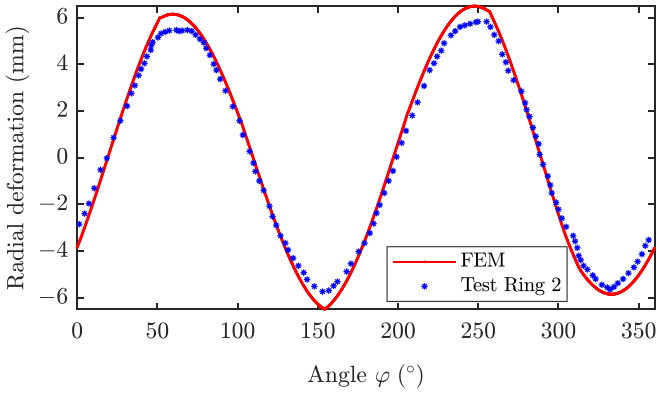


Fig. 12. Comparison between the measurements of the inner radial displacements obtained in the full-scale test (markers in blue) and the ones obtained by the FE analysis (line in red).

## 8 Structural utilization level assessment

For the estimation of the structural utilization level of the lining, it is necessary to designate a physical quantity capable of representing the global structure state. Here, the maximum positive (and negative) bending stresses are selected for the assessment of the lining structural conditions. In fact, the stress state at a certain cross-section in the lining is governed by the combination of the bending and axial components of the stresses. However, since the axial stress component was cleared from the measurements in this study, in order to be able to apply the FNNs to the real input data, the axial components are here neglected. During the experiment, the axial contribution to the measured stresses was removed and only the bending component was provided. However, the approach might be used to predict both the maximum bending action and the corresponding axial force, when the original stress measurement is used (Gottardi et al., 2023a). Similarly to what has been carried out in Section 7, a group of 10 FNNs

Table 6
Performances exhibited by the FNNs on the input data obtained from the FE simulation for both patterns 1 and 2.

| Pattern | Input | Output | $\sigma_{b,77}$ | $\sigma_{b,231}$ | $\sigma_{b,max,pos}$ | $\sigma_{b,max,neg}$ |
|---|---|---|---|---|---|---|
| Pattern 1 | $\sigma_b$ @ 26°, 129°, 179°, 276°, 289° | value (MPa) | 5.387 | 5.738 | 6.339 | −5.651 |
| | | $e_{\%}$ (%) | 9.46 | 22.64 | 19.83 | 11.24 |
| Pattern 2 | $u_r$ @ 27°, 77°, 129°, 232°, 286°, 340° | value (MPa) | 4.926 | 5.151 | 5.943 | −5.828 |
| | | $e_{\%}$ (%) | 0.09 | 10.09 | 12.35 | 14.72 |

has been trained using the same patterns as before, but this time both the maximum positive and negative bending stresses in the structure are predicted. The results of the analysis are shown in Tables 7 and 8.

For a satisfactory accuracy of the network predictions, a more complex architecture has to be employed with respect to the foregoing cases. The mean and standard deviation of the normalized MSE of the networks trained and applied on the synthetic data are computed both for training and testing stage, as it is summarized in Table 7. Additionally, in Table 8, the average predicted maximum (and minimum) bending stresses of the networks along with the standard deviation of the predictions are shown and the absolute and percentage errors with respect to the reference values are calculated. Specifically, the percentage errors for the predictions of the maximum (and minimum) bending stress are computed according to the expression:

$$e_{\%,\max(\min)} = \frac{\left(\frac{1}{10}\sum_{k=1}^{10}\sigma^{\text{pred}}_{k,\max(\min)}\right) - \sigma^{\text{FE}}_{\max(\min)}}{\sigma^{\text{FE}}_{\max(\min)}} \times 100, \tag{5}$$

where the predicted values are compared with the maximum positive and negative bending stresses obtained in the structure in the FE simulation. For both types of input configurations, the errors in the predicted quantities $e_{\%,\max(\min)}$ is less than 10%, achieving acceptable performances especially for the case when the stresses are employed as input, where an error of less than 4% is obtained. It is worth noting that no experimental measurements of the maximum bending stresses were recorded, therefore the network predictions are compared with inferred values obtained from the FE analysis of the plausibility check.

## 9 Conclusions

An innovative method for the structural utilization level assessment of segmental lining based on monitoring data has been presented. The aim was to use monitored data, which are routinely recorded in equipped-monitoring sections and in standard monitoring configurations to avoid loss of generality. The methodological approach is based on a framework, which combines FE analyses and machine learning tools to achieve a real-time prediction of the target quantities. In the study, two main architectures of feed-forward neural networks were examined. In the former, the tangential stresses at specific locations are employed as input data, while in the latter radial displacements are used. A batch of 10 FNNs is created, and by comparing the performances of the neural networks on the synthetic data during training and testing a good accuracy of the predicted stresses at the sought locations has been observed for both neural network configurations.

The results from a full-scale test on segmental lining were employed for the validation of the method. To replicate real application conditions, it was assumed not to

Table 7
Performances exhibited by the FNNs for both patterns 1 and 2 on the synthetic data.

| Pattern | Samples | Arch.[a] | Input [b] | Output | $\mu_{train}$ [c] | $\sigma_{train}$ [c] | $\mu_{test}$ [c] | $\sigma_{test}$ [c] |
|---|---|---|---|---|---|---|---|---|
| Pattern 1 | 4000 | 12–3 | $\sigma_b$ @ 26°, 129°, 179°, 276°, 289° | $\sigma_{b,max,pos}$ $\sigma_{b,min,neg}$ | $5.23 \times 10^{-3}$ | $3.49 \times 10^{-4}$ | $5.59 \times 10^{-3}$ | $4.22 \times 10^{-4}$ |
| Pattern 2 | 4000 | 12–3 | $u_r$ @ 27°, 77°, 129°, 232°, 286° 340° | $\sigma_{b,max,pos}$ $\sigma_{b,min,neg}$ | $2.78 \times 10^{-2}$ | $1.50 \times 10^{-3}$ | $3.61 \times 10^{-2}$ | $4.98 \times 10^{-3}$ |

[a] Architecture: neurons in the hidden layers. Each hidden layer is separated by - sign.
[b] The positions of the input data are specified by the angles $\varphi$ following the @ symbol.
[c] Mean and standard deviation of the normalized MSE during training and testing of the FNNs on the synthetic data.

Table 8
Comparison between the mean predicted values and the actual maximum bending stresses.

| Pattern | $\mu_{pr}$ (MPa) | $\sigma_{pr}$ (MPa) | $e_{abs}$ (MPa) | $e_{\%}$ (%) | Target (MPa) $\sigma_{b,max,pos}$ | Target (MPa) $\sigma_{b,min,neg}$ |
|---|---|---|---|---|---|---|
| Pattern 1 | 5.413 | $1.83 \times 10^{-1}$ | $1.22 \times 10^{-1}$ | 2.32 | 5.29 | |
| | −4.899 | $1.97 \times 10^{-1}$ | $1.81 \times 10^{-1}$ | −3.57 | | −5.08 |
| Pattern 2 | 5.571 | $5.10 \times 10^{-1}$ | $2.81 \times 10^{-1}$ | 5.31 | 5.29 | |
| | −5.559 | $4.33 \times 10^{-1}$ | $-4.79 \times 10^{-1}$ | 9.42 | | −5.08 |

know completely the boundary conditions of the experimental test during the definition of the FE model. For this reason, the lining was assumed to be embedded in the ground while the load was applied as a geostatic stress, instead of directly on the lining. That way, it was possible to test the generality of the developed approach.

The method has been validated with the experiment by employing the measurements as input and by comparing the predicted stresses in the lining with the measured ones. A very good match was obtained both when the stresses were employed as input and when the radial displacements were used. However, when stresses were selected as input better predictions were recorded of $\sigma_{b,77}$ and $\sigma_{b,231}$ than by using the radial displacements, with prediction errors of 0.5% and 3.3% in the former case, and 1.5% and 6.5% in the latter. Another interesting aspect was that the standard deviation of the predicted values of the neural networks in the batch was small, meaning that similar performances for the trained FNNs were achieved. This shows the robustness and the repeatability of the proposed method. In general, FNNs can be trained employing both stresses and displacements as input. However, in this case we need both stress and displacement measurements to predict the stresses at the two sought positions, which is more restrictive. Specifically, the purpose of this manuscript was to investigate the performance of two network patterns, which considered different physical input quantities.

A plausibility analysis of the FE model was also carried out to further verify that the assumptions made in the model are acceptable. The good agreement in the comparison of the radial displacements and the bending stresses obtained in the FE model with the ones measured in the test revealed how the hypotheses assumed could be plausible within a good degree of approximation.

For the actual estimation of the utilization level of the structure, the maximum magnitudes of the bending stress in the lining were designated as suitable indicators. FNNs were trained to predict this quantity starting either from input stresses at certain locations or input radial displacements. The predicted values have been compared with simulated data since no actual maximum stress measurements were recorded in the structure experiment. Satisfactory results were achieved with regard to the predicted maximum bending stresses reached in the lining, showing the possibility of deploying the developed concept for the lining utilization assessment.

A future extension of the method foresees the prediction of the complete stress distribution along the full lining ring to assess the structural safety and reliability, and more advanced FE models to take into account, besides the already considered nonlinear kinematics and the nonlinear behavior of reinforced concrete due to cracks formation. The study presented in this manuscript focused on a new method developed within a research center to help the assessment of the integrity of lining structures in deep tunnels based on a reduced amount of measurements. The framework itself spans over multiple fields, from structural analyses to tunneling and machine learning. Against this background, the authors attempted to create a balanced manuscript among all these fields, providing the necessary information of the main topics addressed to be able to reach a vast community of not only researchers, but also practitioners active in the field of underground constructions. A more specialized study focused on the optimization of the FNN models considering multiple topologies and input–output patterns will be considered for future work.

## Declaration of competing interest

Günther Meschke is an editorial board member for Underground Space and was not involved in the editorial review or the decision to publish this article. All authors declare that there are no competing interests.

## Acknowledgement

This research is funded by the Deutsche Forschungsgemeinschaft (DFG, German Research Foundation, Project No. 77309832) within Subprojects C1 and B2 of the Collaborative Research Center SFB 837 "Interaction Modeling in Mechanised Tunnelling", sited at the Ruhr University Bochum, Germany.

## Appendix A

The combinations of input measurements used for the parametric study on the investigation of the influence of a reduced number of input information on the model predictions is given in Table A1.

Table A1
Sets of input parameters used for each of the two patterns analyzed in the parametric study.

| Number of inputs | Pattern 1 | Pattern 2 |
|---|---|---|
| 1 | $\sigma_b$ @ 26° | $u_r$ @ 27° |
| 2 | $\sigma_b$ @ 26°, 129° | $u_r$ @ 27°, 77° |
| 3 | $\sigma_b$ @ 26°, 129°, 179° | $u_r$ @ 27°, 77°, 129° |
| 4 | $\sigma_b$ @ 26°, 129°, 179°, 276° | $u_r$ @ 27°, 77°, 129°, 232° |
| 5 | – | $u_r$ @ 27°, 77°, 129°, 232°, 286° |

## References


Adeli, H. (2001). Neural networks in civil engineering: 1989–2000. *Computer-Aided Civil and Infrastructure Engineering, 16*, 126–142.

Basheer, I., & Hajmeer, M. (2000). Artificial neural networks: Fundamentals, computing, design, and application. *Journal of Microbiological Methods, 43*, 3–31.

Bishop, C. (2006). *Pattern Recognition and Machine Learning*. Berlin, Heidelberg: Springer-Verlag.

Blom, C. (2002). *Design philosophy of concrete linings for tunnels in soft soils*. [PhD thesis, Delft University].

Blom, C., & van Oosterhout, G. (2001). *Full-scale laboratory tests on a segmented lining* Summary report. Delft University of Technology.

Cao, B., Obel, M., Freitag, S., Heußner, L., Meschke, G., & Mark, P. (2022). Real-time risk assessment of tunneling-induced building damage considering polymorphic uncertainty. *ASCE-ASME Journal of Risk and Uncertainty in Engineering Systems, Part A: Civil Engineering, 8*(1), 04021069.

Cividini, A., Jurina, L., & Gioda, G. (1981). Some aspects of 'characterization' problems in geomechanics. *International Journal of Rock Mechanics and Mining Sciences & Geomechanics Abstracts, 18*(6), 487–503.

Dadvand, P., Rossi, R., & Oñate, E. (2010). An object-oriented environment for developing finite element codes for multi-disciplinary applications. *Archives of Computational Methods in Engineering, 17*, 253–297.

Do, N.-A., Oreste, P., Dias, D., Antonello, C., Djeran-Maigre, I., & Livio, L. (2014). Stress and strain state in the segmental linings during mechanized tunnelling. *Geomechanics and Engineering, 7*(1), 75–85.

Erharter, G., Marcher, T., & Reinhold, C. (2019). Application of artificial neural networks for underground construction – chances and challenges – insights from the bbt exploratory tunnel Ahrental Pfons. *Geomechanics and Tunneling, 12*(5), 472–477.

Fabozzi, S., Bilotta, E., & Russo, G. (2017). Numerical back-calculation of strain measurements from an instrumented segmental tunnel lining. In *EURO:TUN 2017: Proceedings of the IV International Conference on Computational Methods in Tunneling and Subsurface Engineering*, Innsbruck, Austria.

Freitag, S. (2015). Artificial neural networks in structural mechanics. *Computational Technologies Reviews, 12*, 1–26.

French, S. (1995). Uncertainty and imprecision: Modelling and analysis. *The Journal of the Operational Research Society, 46*(1), 70–79.

Gioda, G., & Maier, G. (1980). Direct search solution of an inverse problem in elastoplasticity: Identification of cohesion, friction angle and in situ stress by pressure tunnel tests. *International Journal for Numerical Methods in Engineering, 15*(12), 1823–1848.

Gottardi, N., Freitag, S., & Meschke, G. (2023a). Safety level assessment of segmental lining in rock. In Anagnostou, G., Benardos, A., and Marinos, V., editors, Expanding Underground - Knowledge and Passion to Make a Positive Impact on the World: Proceedings of the ITA-AITES World Tunnel Congress 2023 (WTC 2023), 12–18 May 2023, Athens, Greece, volume 1 of (1st ed.), pages 2693–2700, London. CRC Press.

Gottardi, N., Freitag, S., & Meschke, G. (2023b). Structural stress prediction based on deformations using artificial neural networks trained with artificial noise. In *Proceedings in Applied Mathematics and Mechanics, 22*(1).

Gudzulic, V., Neu, G. E., & Meschke, G. (2020). Numerical analysis of plain and fiber reinforced concrete structures during cyclic loading: Influence of frictional sliding and crack roughness. In *Proceedings in Applied Mathematics and Mechanics,* Wiley-VCH GmbH.

Haykin, S. (1999). *Neural Networks: A Comprehensive Foundation*. Upper Saddle River, NJ, United States: Prentice Hall PTR.

Hellmich, C., Pichler, B., Heissenberger, R., & Moritz, B. (2020). 150 years reliable railway tunnels – extending the hybrid method for the long-term safety assessment. *Geomechanics and Tunnelling, 13*(5), 538–546.

Saadallah, A., Egorov, A., Cao, B.T., Freitag, S., Morik, K., & Meschke, G. (2019). Active learning for accurate settlement prediction using numerical simulations in mechanized tunneling. *Procedia CIRP, 81,*1052–1058.

Sakurai, S. (2017). *Back Analysis in Rock Engineering*. London: CRC Press.

Schäfer, N., Gudzulic, V., Breitenbücher, R., & Meschke, G. (2021). Experimental and numerical investigations on High Performance SFRC: Cyclic tensile loading and fatigue. *Materials., 14*(24), 7593.

Snozzi, L., & Molinari, J.-F. (2013). A cohesive element model for mixed mode loading with frictional contact capability. *International Journal for Numerical Methods in Engineering, 93*(5), 510–526.

Zhang, J.-L., Vida, C., Yuan, Y., Hellmich, C., Mang, H. A., & Pichler, B. (2017). A hybrid analysis method for displacement-monitored segmented circular tunnel rings. *Engineering Structures, 148*(Supplement C), 839–856.

Zhang, J.-L., Schlappal, T., Yuan, Y., Mang, H. A., & Pichler, B. (2019). The influence of interfacial joints on the structural behavior of segmental tunnel rings subjected to ground pressure. *Tunnelling and Underground Space Technology, 84*, 538–556.

Zhang, J., Liu, X., Yuan, Y., Mang, H., & Pichler, B. (2020). Transfer relations: useful basis for computer-aided engineering of circular arch structures. *Engineering Computations*, ahead-of-print.